

Computing the QRPA Level Density with the Finite Amplitude Method

A. Bjelčić^{a,*}, N. Schunck^a

^a*Nuclear and Chemical Science Division, Lawrence Livermore National Laboratory, Livermore, CA 94551, USA*

Abstract

We describe a new algorithm to calculate the vibrational nuclear level density of an atomic nucleus. Fictitious perturbation operators that probe the response of the system are generated by drawing their matrix elements from some probability distribution function. We use the Finite Amplitude Method to explicitly compute the response for each such sample. With the help of the Kernel Polynomial Method, we build an estimator of the vibrational level density and provide the upper bound of the relative error in the limit of infinitely many random samples. The new algorithm can give accurate estimates of the vibrational level density. Since it is based on drawing multiple samples of perturbation operators, its computational implementation is naturally parallel and scales like the number of available processing units.

Keywords: Nuclear level density, Random Phase Approximation, Finite Amplitude Method, Kernel Polynomial Method

1. Introduction

The first attempts to calculate the nuclear level density were based on the statistical model [1, 2, 3, 4]. The formulas for the nuclear level density and spin distribution of excited states that are implemented in modern nuclear reaction codes such as TALYS [5] or EMPIRE [6] are largely based on these early formulations. While such an approach gives the correct asymptotic, it relies on adjustable parameters and usually fails to capture the low-lying, discrete part of the spectrum. Direct methods based on the nuclear shell model are much more predictive but can only be applied in light-to-medium mass nuclei or with schematic interactions [7, 8, 9, 10, 11, 12, 13].

What is often referred to as the combinatorial method is a good compromise between predictive power and feasibility [14]. It is based on the general framework of the nuclear energy density functional theory, where several many-body methods can be leveraged to compute nuclear properties at a reasonable computational cost [15]. The combinatorial method relies on counting nuclear excitations using generating function techniques [16]. In the earlier version of the method, nuclear excited states were computed as n -particle n -holes excitations [14]. The theory was extended to include vibrational and rotational states [17, 18] and the effect of nuclear excitation energy on the single-particle structure [19]. Most recently, particle-hole excitations were replaced by the exact eigenvalues of the Quasiparticle Random Phase (QRPA) matrix, giving a much more realistic description of low-lying states [20].

While the latest version of the combinatorial method contains a lot of new physics, it has become computationally expensive in deformed nuclei, where the QRPA matrix may easily reach sizes of $10^6 \times 10^6$ for realistic harmonic oscillator basis.

Computing all these matrix elements is only doable on a case-by-case basis or with additional approximations such as cut-offs in quasiparticle space or smaller bases [21, 22]. The Finite Amplitude Method (FAM) offers a computationally efficient alternative to computing the QRPA linear response for a given excitation operator without explicitly constructing the QRPA matrix, but does not have direct access to the QRPA eigenfrequencies, i.e. the vibrational spectrum [23, 24].

In this paper, we show that we can still use the Finite Amplitude Method to efficiently probe the vibrational spectrum of nuclei of arbitrary size and compute estimates of the density of phonons with controlled precision.

In Section 2, we summarize very briefly the QRPA and linear response theory to introduce the vibrational level density. Our new solution method is outlined in Section 3. Practical aspects related to its implementation, which requires introducing an additional algorithm known as the Kernel Polynomial Method, are discussed in Section 4. In Section 5, we illustrate the performance of the method with several benchmarks, both with synthetic or realistic data.

2. QRPA level density

In this section, we recall some of the basic properties of the QRPA matrix and of the linear response theory formalism which is used to compute the response of the nucleus to a given excitation operator.

2.1. Notations

Throughout the paper we use A^\dagger for the Hermitian conjugate matrix, A^T for the transposed matrix and A^* for the element-wise complex conjugate matrix of an arbitrary matrix $A \in \mathbb{C}^{m \times n}$. We also use MATLAB notation for diagonal matrices, i.e. if $\mathbf{x} \in \mathbb{C}^n$ is a vector, then $\text{diag}[\mathbf{x}] \in \mathbb{C}^{n \times n}$ is a diagonal matrix having elements of the vector \mathbf{x} as diagonal elements, i.e. $\text{diag}[\mathbf{x}]_{ij} =$

*Corresponding author.

E-mail address: bjelcic1@llnl.gov

$\delta_{ij}x_i$, for $i, j = 1, \dots, n$. For a matrix $A \in \mathbb{C}^{m \times n}$, the Frobenius norm is denoted by: $\|A\|_F = \sqrt{\sum_{i=1}^m \sum_{j=1}^n |A_{ij}|^2}$, while the Euclidean norm of a vector $\mathbf{v} \in \mathbb{C}^n$ is $\|\mathbf{v}\| = \sqrt{\sum_{i=1}^n |v_i|^2}$. We denote the imaginary unit as i . For an n -dimensional random vector \mathbf{X} that follows the multivariate Gaussian distribution with expected value $\boldsymbol{\mu} \in \mathbb{R}^n$ and covariance matrix $\Sigma \in \mathbb{R}^{n \times n}$, we use the notation: $\mathbf{X} \sim \mathcal{N}_n(\boldsymbol{\mu}, \Sigma)$. For a random variable X , $\mathbb{E}[X]$ is its expected mean value and $\text{Var}(X)$ its variance.

2.2. QRPA matrix

The goal of this paper is to compute the QRPA level density function $\rho(\omega)$, for all $\omega \geq 0$, defined as

$$\rho(\omega) = \sum_{i=1}^{N_p} \delta(\omega - \Omega_i), \quad (1)$$

where $N_p \in \mathbb{N}$ is the number of quasiparticle pairs $\mu < \nu$, and the Ω_i are the QRPA eigenfrequencies defined as the positive eigenvalues of the QRPA matrix \mathcal{S}

$$\mathcal{S} = \begin{bmatrix} +I & \mathbf{0} \\ \mathbf{0} & -I \end{bmatrix} \begin{bmatrix} A & B \\ B^* & A^* \end{bmatrix}, \quad (2)$$

where the matrices $A, B \in \mathbb{C}^{N_p \times N_p}$ satisfy $A^\dagger = A$ and $B^T = B$ and involve the second derivatives of the energy functional with respect to the normal and pairing densities [15, 25]. It is customary to introduce the QRPA eigenmodes $X, Y \in \mathbb{C}^{N_p \times N_p}$ to define the eigenvectors of the QRPA matrix. If $\Omega = \text{diag}[\Omega_i]_{i=1}^{N_p} \in \mathbb{R}^{N_p \times N_p}$ is the diagonal matrix made of its eigenvalues and is such that $\Omega_i > 0$ for each $i = 1, \dots, N_p$, then one can show that

$$\begin{bmatrix} +I & \mathbf{0} \\ \mathbf{0} & -I \end{bmatrix} \begin{bmatrix} A & B \\ B^* & A^* \end{bmatrix} = \begin{bmatrix} X & Y^* \\ Y & X^* \end{bmatrix} \begin{bmatrix} +\Omega & \mathbf{0} \\ \mathbf{0} & -\Omega \end{bmatrix} \begin{bmatrix} X & Y^* \\ Y & X^* \end{bmatrix}^{-1}, \quad (3)$$

with

$$\begin{bmatrix} X & Y^* \\ Y & X^* \end{bmatrix}^{-1} = \begin{bmatrix} +I & \mathbf{0} \\ \mathbf{0} & -I \end{bmatrix} \begin{bmatrix} X & Y^* \\ Y & X^* \end{bmatrix}^\dagger \begin{bmatrix} +I & \mathbf{0} \\ \mathbf{0} & -I \end{bmatrix}. \quad (4)$$

In the context of numerical linear algebra, the function $\rho(\omega)$ is known as the spectral density of the QRPA matrix \mathcal{S} . The practical calculation of this function in the case of the QRPA matrix (2) faces two problems

- In spherical nuclei, the QRPA matrix \mathcal{S} can be easily constructed and diagonalized as in Eqs. (3) and (4). In that case, one has an explicit access to the QRPA eigenfrequencies $\{\Omega_i\}_{i=1}^{N_p}$, and therefore the computation of the level density function $\rho(\omega)$ becomes trivial. However, in heavy deformed nuclei the dimension N_p becomes prohibitively large as it can reach $N_p \sim 10^6$ for large harmonic oscillator bases. In those cases, the direct determination and diagonalization of the QRPA matrix has only been achieved in a few cases [21, 22].
- Although numerous numerical methods for estimating the spectral density exist [26, 27], they all assume that the

matrix for which the spectral density is computed is Hermitian. In our case, the QRPA matrix \mathcal{S} is not Hermitian and the matrix of its eigenvectors is not unitary but involves the orthonormality condition of Eq. (4). Therefore, those spectral density methods cannot be directly used.

2.3. Linear response theory

While the QRPA approximation is the small amplitude limit of the time-dependent Hartree-Fock-Bogoliubov theory, linear response theory is the same limit in the presence of an external, time-dependent field $\hat{F}(t)$ [25]. In the quasiparticle basis represented by the quasiparticle creation and annihilation operators $\hat{\beta}_\mu^\dagger$ and $\hat{\beta}_\nu$, this field is represented as [15]

$$\hat{F} = \frac{1}{2} \sum_{\mu\nu} \left[F_{\mu\nu}^{11} \hat{\beta}_\mu^\dagger \hat{\beta}_\nu + F_{\mu\nu}^{20} \hat{\beta}_\mu^\dagger \hat{\beta}_\nu^\dagger + F_{\mu\nu}^{02} \hat{\beta}_\mu \hat{\beta}_\nu - F_{\mu\nu}^{11*} \hat{\beta}_\mu \hat{\beta}_\nu^\dagger \right]. \quad (5)$$

Let $F^{20}, F^{02} \in \mathbb{C}^{N_p}$ be the vectorized strict upper triangle parts ($\mu < \nu$) of the matrices $F_{\mu\nu}^{20}, F_{\mu\nu}^{02}$. For $\omega \in \mathbb{R}$ and smearing $\gamma > 0$, we denote the complex frequency $\omega_\gamma = \omega + \gamma i$ in the upper complex plane.

In the small amplitude limit, the external perturbation induces oscillations of the Hamiltonian $\delta H_{\mu\nu}^{20}(\omega_\gamma)$ and $\delta H_{\mu\nu}^{02}(\omega_\gamma)$ according to the equations [24],

$$\begin{aligned} (E_\mu + E_\nu - \omega_\gamma) X_{\mu\nu}(\omega_\gamma) + \delta H_{\mu\nu}^{20}(\omega_\gamma) &= F_{\mu\nu}^{20}(\omega_\gamma), \\ (E_\mu + E_\nu + \omega_\gamma) Y_{\mu\nu}(\omega_\gamma) + \delta H_{\mu\nu}^{02}(\omega_\gamma) &= F_{\mu\nu}^{02}(\omega_\gamma), \end{aligned} \quad (6)$$

where the antisymmetric matrices $X_{\mu\nu}(\omega)$ and $Y_{\mu\nu}(\omega)$ are the corresponding forward and backward amplitudes. Let the vectors $X(\omega_\gamma), Y(\omega_\gamma) \in \mathbb{C}^{N_p}$ denote the vectorized strict upper triangle parts of the matrices $X_{\mu\nu}(\omega_\gamma), Y_{\mu\nu}(\omega_\gamma)$. By expanding $\delta H_{\mu\nu}^{20}(\omega_\gamma)$ and $\delta H_{\mu\nu}^{02}(\omega_\gamma)$ in terms of the amplitudes $X_{\mu\nu}(\omega_\gamma)$ and $Y_{\mu\nu}(\omega_\gamma)$ we obtain the linear response equation,

$$\begin{bmatrix} A & B \\ B^* & A^* \end{bmatrix} - \omega_\gamma \begin{bmatrix} +I & \mathbf{0} \\ \mathbf{0} & -I \end{bmatrix} \begin{bmatrix} X(\omega_\gamma) \\ Y(\omega_\gamma) \end{bmatrix} = - \begin{bmatrix} F^{20} \\ F^{02} \end{bmatrix}. \quad (7)$$

Traditionally, Eq. (7) is solved by explicitly constructing and diagonalizing the matrix \mathcal{S} of Eq. (2), which can become computationally prohibitive for heavy deformed nuclei. However, it is in fact possible to solve for the $X(\omega_\gamma)$ and $Y(\omega_\gamma)$ without having to compute the matrix elements of \mathcal{S} using the Finite Amplitude Method (FAM) [23, 24]. The key idea of the FAM is to iteratively solve Eq. (6), independently for each frequency ω on a chosen mesh. As was shown in Ref. [28], the FAM actually only accesses the mapping

$$\begin{bmatrix} x \\ y \end{bmatrix} \in \mathbb{C}^{2N_p} \mapsto \begin{bmatrix} A & B \\ B^* & A^* \end{bmatrix} \begin{bmatrix} x \\ y \end{bmatrix} \in \mathbb{C}^{2N_p}, \quad (8)$$

and therefore the FAM could be classified as a matrix-free method for solving the linear system (7). In the rest of this paper, we will make extensive use of this property and design a method to estimate the spectral density $\rho(\omega)$ by only using the mapping (8).

For any given operator \hat{F} , we define the strength function $S(\omega_\gamma, \hat{F})$ as

$$S(\omega_\gamma, \hat{F}) = \begin{bmatrix} F^{20} \\ F^{02} \end{bmatrix}^\dagger \begin{bmatrix} X(\omega_\gamma) \\ Y(\omega_\gamma) \end{bmatrix}, \quad (9)$$

and the response function $dB(\omega, \hat{F})/d\omega$ as

$$\frac{dB(\omega, \hat{F})}{d\omega} = \lim_{\gamma \rightarrow 0^+} \frac{-1}{\pi} \text{Im} [S(\omega_\gamma, \hat{F})]. \quad (10)$$

One can show that the response function can be written as

$$\frac{dB(\omega, \hat{F})}{d\omega} = \sum_{i=1}^{N_p} |\langle i|\hat{F}|0\rangle|^2 \delta(\omega - \Omega_i) - \sum_{i=1}^{N_p} |\langle 0|\hat{F}|i\rangle|^2 \delta(\omega + \Omega_i), \quad (11)$$

where $|0\rangle$ is the QRPA ground state, and $|i\rangle = \hat{O}_i^\dagger |0\rangle$ is the i -th excited state defined from the phonon creation operators \hat{O}_i^\dagger

$$\hat{O}_i^\dagger = \sum_{\mu < \nu} [X_{\mu\nu}^i \hat{\beta}_\mu^\dagger \hat{\beta}_\nu^\dagger - Y_{\mu\nu}^i \hat{\beta}_\nu \hat{\beta}_\mu]. \quad (12)$$

Using Eqs. (5) and (12) we can compute the transition strengths [29]

$$\begin{aligned} T_i(\hat{F}) &= \langle i|\hat{F}|0\rangle = \langle \Phi_0 | [\hat{O}_i, \hat{F}] | \Phi_0 \rangle = \sum_{\mu < \nu} [(X_{\mu\nu}^i)^* F_{\mu\nu}^{20} + (Y_{\mu\nu}^i)^* F_{\mu\nu}^{02}], \\ \tilde{T}_i(\hat{F}) &= \langle 0|\hat{F}|i\rangle = \langle \Phi_0 | [\hat{O}_i^\dagger, \hat{F}] | \Phi_0 \rangle = \sum_{\mu < \nu} [Y_{\mu\nu}^i F_{\mu\nu}^{20} + X_{\mu\nu}^i F_{\mu\nu}^{02}], \end{aligned} \quad (13)$$

where $|\Phi_0\rangle$ is the HFB state. A shorthand, vectorized form of these transition strengths reads

$$\begin{bmatrix} T(\hat{F}) \\ \tilde{T}(\hat{F}) \end{bmatrix} = \begin{bmatrix} X & Y^* \\ Y & X^* \end{bmatrix}^\dagger \begin{bmatrix} F^{20} \\ F^{02} \end{bmatrix}. \quad (14)$$

Using Eq. (4), we can also invert the previous equation:

$$\begin{bmatrix} F^{20} \\ F^{02} \end{bmatrix} = \begin{bmatrix} +\mathbf{I} & \mathbf{0} \\ \mathbf{0} & -\mathbf{I} \end{bmatrix} \begin{bmatrix} X & Y^* \\ Y & X^* \end{bmatrix} \begin{bmatrix} +\mathbf{I} & \mathbf{0} \\ \mathbf{0} & -\mathbf{I} \end{bmatrix} \begin{bmatrix} T(\hat{F}) \\ \tilde{T}(\hat{F}) \end{bmatrix}. \quad (15)$$

Notice that if we choose the excitation operator \hat{F}' (i.e. picked $F_{\mu,\nu}^{\prime 20}, F_{\mu,\nu}^{\prime 02} \in \mathbb{C}$) such that

$$\begin{bmatrix} +F^{\prime 20} \\ -F^{\prime 02} \end{bmatrix} = \begin{bmatrix} X & Y^* \\ Y & X^* \end{bmatrix} \begin{bmatrix} \mathbf{1} \\ \mathbf{1} \end{bmatrix}, \quad (16)$$

where $\mathbf{1} = [1, \dots, 1]^T \in \mathbb{R}^{N_p}$, then we would have:

$$|T_i(\hat{F}')|^2 = |\langle i|\hat{F}'|0\rangle|^2 = 1 \quad \text{and} \quad |\tilde{T}_i(\hat{F}')|^2 = |\langle 0|\hat{F}'|i\rangle|^2 = 1, \quad (17)$$

for all $i = 1, \dots, N_p$, and consequently the response function for that specific operator \hat{F}' would be equal to the QRPA level density function

$$\frac{dB(\omega, \hat{F}')}{d\omega} = \rho(\omega), \quad \forall \omega \geq 0. \quad (18)$$

In practice, such operator \hat{F}' is impossible to construct because it essentially involves computing the sum of all eigenvectors

in Eq. (16), and therefore requires the full diagonalization of the QRPA matrix. However, this simple example demonstrates that by carefully picking the excitation operator and afterwards solving only the linear response equation (7), one can, at least in principle, obtain an approximation of the QRPA level density function. Therefore, the main question is how to efficiently construct an operator \hat{F}' which excites all the eigenmodes with equal strength.

3. Method description

We consider a collection of N_s random excitation operators \hat{F}_{i_s} , for $1 \leq i_s \leq N_s$, with matrix elements $F_{i_s}^{20}, F_{i_s}^{02}$ drawn from a multivariate Gaussian distribution. We will show how to estimate the QRPA level density function $\rho(\omega)$ by introducing a specific averaging procedure over the collection of the obtained response functions $dB(\omega, \hat{F}_{i_s})/d\omega$ computed for each sample operator. Before we proceed, we recall a well-known Lemma describing how a Gaussian random vector is affected by a linear transformation.

Lemma 3.1. *Let $\mathbf{X} \sim \mathcal{N}_n(\mathbf{0}, \Sigma)$ be a n -dimensional random vector having multivariate Gaussian distribution with zero expected value and covariance matrix Σ . Then for any matrix $A \in \mathbb{R}^{m \times n}$, the m -dimensional random vector $A\mathbf{X}$ has a multivariate Gaussian distribution with zero expected value and covariance matrix $A\Sigma A^T$, i.e. $A\mathbf{X} \sim \mathcal{N}_m(\mathbf{0}, A\Sigma A^T)$.*

3.1. Randomized excitation operator

According to Theorem 1. in Appendix B from Ref. [28], there exist $C, D \in \mathbb{C}^{N_p \times N_p}$ unitary matrices and diagonal matrix $\theta = \text{diag}[\theta_i]_{i=1}^{N_p}$, for $\theta_1, \dots, \theta_{N_p} \geq 0$, such that

$$X = D \cosh \theta C \quad \text{and} \quad Y = D^* \sinh \theta C. \quad (19)$$

Inserting the previous relations into Eq. (14), we obtain:

$$\begin{aligned} \begin{bmatrix} T(\hat{F}) \\ \tilde{T}(\hat{F}) \end{bmatrix} &= \begin{bmatrix} X & Y^* \\ Y & X^* \end{bmatrix}^\dagger \begin{bmatrix} F^{20} \\ F^{02} \end{bmatrix} \\ &= \begin{bmatrix} C^\dagger & \mathbf{0} \\ \mathbf{0} & C^T \end{bmatrix} \begin{bmatrix} \cosh \theta & \sinh \theta \\ \sinh \theta & \cosh \theta \end{bmatrix} \begin{bmatrix} D^\dagger & \mathbf{0} \\ \mathbf{0} & D^T \end{bmatrix} \begin{bmatrix} F^{20} \\ F^{02} \end{bmatrix}. \end{aligned} \quad (20)$$

Suppose that $F^{20}, F^{02} \in \mathbb{C}^{N_p}$ are random complex vectors, such that all the components

$$\text{Re}[F_i^{20}], \text{Re}[F_i^{02}], \text{Im}[F_i^{20}], \text{Im}[F_i^{02}] \sim \mathcal{N}_1(0, \sigma^2), \quad (21)$$

are independent and identically distributed Gaussian random variables with zero expected value and the same variance $\sigma^2 > 0$, for each $i = 1, \dots, N_p$. Then it is easy to show that the $4N_p$ -dimensional random vector

$$\begin{bmatrix} \text{Re } F^{20} \\ \text{Re } F^{02} \\ \text{Im } F^{20} \\ \text{Im } F^{02} \end{bmatrix} \sim \mathcal{N}_{4N_p}(\mathbf{0}, \sigma^2 \mathbf{I}), \quad (22)$$

has multivariate Gaussian distribution with zero expected value and covariance matrix $\sigma^2 \mathbf{I}$.

Let us introduce the real and imaginary parts: $C_1, C_2, D_1, D_2 \in \mathbb{R}^{N_p \times N_p}$ of C and D matrices, i.e. $C = C_1 + C_2 i$ and $D = D_1 + D_2 i$. It is easy to see that Eq. (20) can be recast into

$$\begin{bmatrix} \text{Re } T(\hat{F}) \\ \text{Re } \tilde{T}(\hat{F}) \\ \text{Im } T(\hat{F}) \\ \text{Im } \tilde{T}(\hat{F}) \end{bmatrix} = \mathcal{X} \begin{bmatrix} \text{Re } F^{20} \\ \text{Re } F^{02} \\ \text{Im } F^{20} \\ \text{Im } F^{02} \end{bmatrix}, \quad (23)$$

where the real matrix $\mathcal{X} \in \mathbb{R}^{4N_p \times 4N_p}$ is given by

$$\mathcal{X} = C \begin{bmatrix} \cosh \theta & \sinh \theta & \mathbf{0} & \mathbf{0} \\ \sinh \theta & \cosh \theta & \mathbf{0} & \mathbf{0} \\ \mathbf{0} & \mathbf{0} & \cosh \theta & \sinh \theta \\ \mathbf{0} & \mathbf{0} & \sinh \theta & \cosh \theta \end{bmatrix} \mathcal{D}, \quad (24)$$

with

$$C = \begin{bmatrix} C_1^T & \mathbf{0} & C_2^T & \mathbf{0} \\ \mathbf{0} & C_1^T & \mathbf{0} & -C_2^T \\ -C_2^T & \mathbf{0} & C_1^T & \mathbf{0} \\ \mathbf{0} & C_2^T & \mathbf{0} & C_1^T \end{bmatrix} \quad (25)$$

$$\mathcal{D} = \begin{bmatrix} D_1^T & \mathbf{0} & D_2^T & \mathbf{0} \\ \mathbf{0} & D_1^T & \mathbf{0} & -D_2^T \\ -D_2^T & \mathbf{0} & D_1^T & \mathbf{0} \\ \mathbf{0} & D_2^T & \mathbf{0} & D_1^T \end{bmatrix}. \quad (26)$$

Both matrices C and \mathcal{D} are orthogonal since C and D are unitary.

According to Lemma 3.1, we know that the following $4N_p$ -dimensional random vector,

$$\begin{bmatrix} \text{Re } T(\hat{F}) \\ \text{Re } \tilde{T}(\hat{F}) \\ \text{Im } T(\hat{F}) \\ \text{Im } \tilde{T}(\hat{F}) \end{bmatrix} \sim \mathcal{N}_{4N_p}(\mathbf{0}, \Sigma), \quad (27)$$

has multivariate Gaussian distribution with zero expected value and (real) covariance matrix $\Sigma = \mathcal{X}(\sigma^2 \mathbf{I})\mathcal{X}^T$. We can easily extract an arbitrary component of the random vector (27). As an example, for any $j = 1, \dots, N_p$, we have

$$\text{Re } T_j(\hat{F}) \equiv \text{Re}[\langle j|\hat{F}|0\rangle] = \begin{bmatrix} \mathbf{e}_j \\ \mathbf{0} \\ \mathbf{0} \\ \mathbf{0} \end{bmatrix}^T \begin{bmatrix} \text{Re } T(\hat{F}) \\ \text{Re } \tilde{T}(\hat{F}) \\ \text{Im } T(\hat{F}) \\ \text{Im } \tilde{T}(\hat{F}) \end{bmatrix}. \quad (28)$$

Invoking Lemma 3.1 again, we see that the random variable $\text{Re}[\langle j|\hat{F}|0\rangle] \sim \mathcal{N}(0, \sigma_j^2)$ has Gaussian distribution with zero expected value and variance σ_j^2 given by

$$\sigma_j^2 = \begin{bmatrix} \mathbf{e}_j \\ \mathbf{0} \\ \mathbf{0} \\ \mathbf{0} \end{bmatrix}^T \Sigma \begin{bmatrix} \mathbf{e}_j \\ \mathbf{0} \\ \mathbf{0} \\ \mathbf{0} \end{bmatrix}. \quad (29)$$

Using the result $\Sigma = \mathcal{X}(\sigma^2 \mathbf{I})\mathcal{X}^T$, this can be easily be computed explicitly as

$$\sigma_j^2 = \sigma^2 + 2\sigma^2 \|Y\mathbf{e}_j\|^2. \quad (30)$$

Repeating a similar procedure for the other components of the random vector (27), we find that for any $i = 1, \dots, N_p$,

$$\text{Re}[\langle i|\hat{F}|0\rangle], \text{Re}[\langle 0|\hat{F}|i\rangle], \text{Im}[\langle i|\hat{F}|0\rangle], \text{Im}[\langle 0|\hat{F}|i\rangle] \sim \mathcal{N}_1(0, \sigma_i^2) \quad (31)$$

with the variance σ_i^2 given by Eq. (30). It is worth mentioning that all these components are not necessarily independent random variables.

We can now for any $i = 1, \dots, N_p$ compute the following expected value

$$\mathbb{E}[\langle i|\hat{F}|0\rangle^2] = \mathbb{E}[\text{Re}[\langle i|\hat{F}|0\rangle]^2] + \mathbb{E}[\text{Im}[\langle i|\hat{F}|0\rangle]^2]. \quad (32)$$

Since for any random variable X with zero expected value its variance can be expressed as $\text{Var}(X) = \mathbb{E}[X^2]$, result (31) yields:

$$\mathbb{E}[\langle i|\hat{F}|0\rangle^2] = \sigma_i^2 + \sigma_i^2 = 2\sigma^2 + 4\sigma^2 \|Y\mathbf{e}_i\|^2.$$

The same procedure can be repeated for $\langle 0|\hat{F}|i\rangle^2$. Overall, we conclude that if one draws the elements of F^{20} and F^{02} from a Gaussian distribution as in Eq. (21), then for any $i = 1, \dots, N_p$ there holds:

$$\mathbb{E}[\langle i|\hat{F}|0\rangle^2] = \mathbb{E}[\langle 0|\hat{F}|i\rangle^2] = 4\sigma^2 \left(\frac{1}{2} + \|Y\mathbf{e}_i\|^2 \right). \quad (33)$$

3.2. Level density estimator

Recall that the response function expression (11) for non-negative frequencies $\omega \geq 0$ reads

$$\frac{dB(\omega \geq 0, \hat{F})}{d\omega} = \sum_{i=1}^{N_p} \langle i|\hat{F}|0\rangle^2 \delta(\omega - \Omega_i). \quad (34)$$

Notice that now the response function is a random variable because the excitation operator \hat{F} is a random variable. Also notice that the following integral over non-negative frequencies

$$\int_0^{+\infty} \frac{dB(\omega' \geq 0, \hat{F})}{d\omega'} d\omega' = \sum_{i=1}^{N_p} \langle i|\hat{F}|0\rangle^2, \quad (35)$$

is also a random variable.

Since both random variables in Eqs. (34) and (35) are well defined, we can compute their expected values. Therefore, we can define the QRPA level density estimator $\widehat{\rho}(\omega)$, for non-negative frequencies $\omega \geq 0$, as

$$\widehat{\rho}(\omega) = N_p \frac{\mathbb{E} \left[\frac{dB(\omega \geq 0, \hat{F})}{d\omega} \right]}{\mathbb{E} \left[\int_0^{+\infty} \frac{dB(\omega' \geq 0, \hat{F})}{d\omega'} d\omega' \right]}. \quad (36)$$

Inserting Eq. (33) into Eq. (34) and Eq. (35), we get

$$\mathbb{E} \left[\frac{dB(\omega \geq 0, \hat{F})}{d\omega} \right] = 4\sigma^2 \sum_{i=1}^{N_p} \left(\frac{1}{2} + \|Y\mathbf{e}_i\|^2 \right) \delta(\omega - \Omega_i). \quad (37)$$

and

$$\mathbb{E} \left[\int_0^{+\infty} \frac{dB(\omega' \geq 0, \hat{F})}{d\omega'} d\omega' \right] = 4\sigma^2 N_p \left(\frac{1}{2} + \frac{\|Y\|_F^2}{N_p} \right). \quad (38)$$

Now we can express the estimator $\widehat{\rho}(\omega)$ as

$$\widehat{\rho}(\omega) = \sum_{i=1}^{N_p} \left(\frac{\frac{1}{2} + \|Y\mathbf{e}_i\|^2}{\frac{1}{2} + \frac{\|Y\|_F^2}{N_p}} \right) \delta(\omega - \Omega_i). \quad (39)$$

In the interpretation where the Dirac delta function is a non-negative function of infinitesimal width and unit area, we can easily show that the absolute error $|\widehat{\rho}(\omega) - \rho(\omega)|$ with respect to the true QRPA level density (1) is bounded as

$$|\widehat{\rho}(\omega) - \rho(\omega)| \leq \rho(\omega) \max_{i=1, \dots, N_p} \varepsilon_i, \quad (40)$$

with

$$\varepsilon_i = \left| \frac{\|Y\mathbf{e}_i\|^2 - \frac{\|Y\|_F^2}{N_p}}{\frac{1}{2} + \frac{\|Y\|_F^2}{N_p}} \right|. \quad (41)$$

The relative error bound for any $\omega \geq 0$ is then

$$\left| \frac{\widehat{\rho}(\omega) - \rho(\omega)}{\rho(\omega)} \right| \leq \max_{i=1, \dots, N_p} \varepsilon_i. \quad (42)$$

Assuming for simplicity that the eigenfrequencies Ω_i are non degenerate, we see that as one approaches the given QRPA eigenfrequency $\omega \rightarrow \Omega_i$, the local relative error is

$$\lim_{\omega \rightarrow \Omega_i} \left| \frac{\widehat{\rho}(\omega) - \rho(\omega)}{\rho(\omega)} \right| = \varepsilon_i, \quad \forall i = 1, \dots, N_p. \quad (43)$$

It is worth emphasizing that (42) and (43) hold only approximately if the Dirac delta function is approximated by a finite width function.

If we imagine the level density function $\rho(\omega)$ as the linear response function with all transition probabilities being equal to one, we can see that the level density estimator $\widehat{\rho}(\omega)$ is the linear response function with the proper QRPA eigenfrequencies Ω_i but transition probabilities with relative error bounded by ε_i for each Ω_i . We also notice that ε_i is a measure of how much the squared norm of the i -th column of the Y matrix deviates from the average value over all columns. In practice, the norm $\|Y\|_F$ is relatively small because the matrix Y describes the ground-state correlations [25]. If we expand the residual interaction $\delta H_{\mu\nu}^{20}$ and $\delta H_{\mu\nu}^{02}$ in terms amplitudes $X_{\mu\nu}$ and $Y_{\mu\nu}$:

$$\begin{aligned} \delta H_{\mu\nu}^{20} &= -(E_\mu + E_\nu)X_{\mu\nu} + \sum_{\mu' < \nu'} \left[A_{\mu\nu, \mu'\nu'} X_{\mu'\nu'} + B_{\mu\nu, \mu'\nu'} Y_{\mu'\nu'} \right], \\ \delta H_{\mu\nu}^{02} &= -(E_\mu + E_\nu)Y_{\mu, \nu} + \sum_{\mu' < \nu'} \left[B_{\mu\nu, \mu'\nu'}^* X_{\mu'\nu'} + A_{\mu\nu, \mu'\nu'}^* Y_{\mu'\nu'} \right], \end{aligned} \quad (44)$$

and assume that the residual interaction is relatively weak, i.e., $|\delta H_{\mu\nu}^{20}| \ll 1$ and $|\delta H_{\mu\nu}^{02}| \ll 1$ in addition to ground-state correlations being small ($\|Y\|_F \ll 1$), the QRPA matrix can be simplified to

$$A_{\mu\nu, \mu'\nu'} \approx (E_\mu + E_\nu) \delta_{\mu\nu, \mu'\nu'}, \quad (45)$$

$$B_{\mu\nu, \mu'\nu'} \approx 0, \quad (46)$$

which is known as the cranking approximation. In this case, the QRPA eigenproblem (3) has a trivial solution: $X = \mathbf{I}, Y = \mathbf{0}$, and all the relative errors ε_i are identically equal to zero. If instead we assume $B_{\mu\nu, \mu'\nu'} \approx 0$ while retaining the full matrix A , then the QRPA eigenproblem (3) again has a trivial solution: $X = Q, Y = \mathbf{0}$, where the unitary matrix $Q \in \mathbb{C}^{N_p \times N_p}$ diagonalizes the Hermitian matrix: $A = Q\Lambda Q^\dagger$. The relative errors ε_i are then again zero. Because A has dominant diagonal elements $E_\mu + E_\nu$, we can expect that the eigenvectors $Y_{\mu, \nu}^i$ will be generally small in magnitude, except for a few modes with small eigenfrequencies Ω_i for which the diagonal elements $E_\mu + E_\nu$ are relatively small. This is the reason why we can *a priori* expect very small relative errors ε_i , for all $i = 1, \dots, N_p$, except for a few low-lying modes, and, therefore, why the introduced estimator $\widehat{\rho}(\omega)$ is believed to be a sufficiently good approximation of $\rho(\omega)$.

4. Practical aspects

4.1. Sampling the level density estimator

In practice, random variables can only be sampled, and the expected values in Eq. (36) can be estimated by computing average values over a collection of samples. If we generate a collection of N_s samples of complex vectors $F_{i_s}^{20}, F_{i_s}^{02} \in \mathbb{C}^{N_p}$, for $i_s = 1, \dots, N_s$, such that their real and imaginary parts are independently drawn from a Gaussian distribution with zero expected value and variance σ^2 as in Eq. (22), and if for each of those generated excitation operators \hat{F}_{i_s} we compute the response function $dB/d\omega(\omega, \hat{F}_{i_s})$ on the positive frequencies domain $\omega \geq 0$, then we can approximate the level density estimator (36) as

$$\widehat{\rho}(\omega) = N_p \frac{\frac{1}{N_s} \sum_{i_s=1}^{N_s} \frac{dB(\omega \geq 0, \hat{F}_{i_s})}{d\omega}}{\frac{1}{N_s} \sum_{i_s=1}^{N_s} \int_0^{+\infty} \frac{dB(\omega' \geq 0, \hat{F}_{i_s})}{d\omega'} d\omega'}. \quad (47)$$

Notice that the denominator in the previous equation is an average over all zeroth moments $m_0(\hat{F}_{i_s})$. Of course, the larger the sample size N_s , the better the approximation but the approximation of the level density function does not depend on the variance σ^2 . In principle, one can select any value; in practice, a reasonable choice is to take $\sigma \approx 1$, in whichever measuring unit we express the excitation operator \hat{F} . It is worth mentioning that (42) and (43) hold in the $N_s \rightarrow +\infty$ limit where the expected value matches the computed average value from the collection of samples.

4.2. Kernel Polynomial Method

The estimator (47) seems very practical at first, since any method which can evaluate the response function $dB/d\omega(\omega, \hat{F})$ for an arbitrary excitation operator \hat{F} , as well as the integral in the denominator of Eq. (47) is applicable. For example, one can solve the classical point-by-point FAM equations to compute the numerator on a fine ω grid with small smearing

γ , or use the iterative Arnoldi method from Ref. [30]. The denominator can be evaluated by employing a contour integration technique, as presented in Ref. [29]. However this calculation needs to be performed both over a very large ω domain with small smearing γ and for sufficiently large sample size N_s . As a result, the computational cost of the method could become prohibitive. This issue can be largely mitigated by employing the Kernel Polynomial Method (KPM) introduced in Ref. [28]. The KPM is specifically designed to efficiently compute the response function over the entire $\omega \geq 0$ region of interest for arbitrary excitation operator. In the following we briefly introduce the KPM method and apply it to evaluate the expression in Eq. (47).

We define the bounding frequency Ω_b , such that all the QRPA eigenmodes are contained within the interval: $\Omega_i \subseteq \langle 0, +\Omega_b \rangle$. The main idea of the KPM method is to expand the response function in Chebyshev series

$$\frac{dB^{(\text{KPM})}(\omega, \hat{F})}{d\omega} = \frac{2/\pi}{\Omega_b \sqrt{1 - (\omega/\Omega_b)^2}} \sum_{n=0}^{2N_{\text{it}}} \mu_n(\hat{F}) T_n\left(\frac{\omega}{\Omega_b}\right), \quad (48)$$

where the coefficients $\{\mu_n(\hat{F})\}_{n=0}^{2N_{\text{it}}}$ are computed via the recursive relations given in Ref. [28]. The computation of coefficients $\{\mu_n(\hat{F})\}_{n=0}^{2N_{\text{it}}}$ requires exactly N_{it} evaluations of the QRPA mapping (8). In order to damp the Gibbs oscillations, one needs to multiply these coefficients with the kernel coefficients $\{g_n^{(2N_{\text{it}}+1)}\}_{n=0}^{2N_{\text{it}}}$: $\mu_n(\hat{F}) \leftarrow g_n^{(2N_{\text{it}}+1)} \mu_n(\hat{F})$. In this paper, we use the Jackson kernel [28] unless stated otherwise. Then, the obtained KPM response function is approximately equal to

$$\begin{aligned} \frac{dB^{(\text{KPM})}(\omega, \hat{F})}{d\omega} \approx & + \sum_{i=1}^{N_p} |\langle i|\hat{F}|0\rangle|^2 \delta_{\sigma_{\text{KPM}}}(\omega - \Omega_i) \\ & - \sum_{i=1}^{N_p} |\langle 0|\hat{F}|i\rangle|^2 \delta_{\sigma_{\text{KPM}}}(\omega + \Omega_i), \end{aligned} \quad (49)$$

where $\delta_{\sigma_{\text{KPM}}}(\omega)$ is the Gaussian function:

$$\delta_{\sigma_{\text{KPM}}}(\omega) = \frac{1}{\sqrt{2\pi}\sigma_{\text{KPM}}} \exp\left(-\frac{1}{2} \frac{\omega^2}{\sigma_{\text{KPM}}^2}\right) \quad (50)$$

of width σ_{KPM}

$$\sigma_{\text{KPM}} = \Omega_b \frac{\pi}{2N_{\text{it}} + 1}. \quad (51)$$

The number N_{it} of KPM iterations is determined by the desired resolution σ_{KPM} according to Eq.(51). In the limit $N_{\text{it}} \rightarrow +\infty$, we have indeed: $dB^{(\text{KPM})}/d\omega \rightarrow dB/d\omega$. It is not difficult to see that the zeroth moment $m_0(\hat{F})$ of (48) is

$$m_0(\hat{F}) = \int_0^{+\Omega_b} \frac{dB^{(\text{KPM})}(\omega', \hat{F})}{d\omega'} d\omega' = \sum_{n=0}^{2N_{\text{it}}} \mu_n(\hat{F}) \frac{\sin\left(\frac{n\pi}{2}\right)}{\left(\frac{n\pi}{2}\right)}. \quad (52)$$

In order to evaluate the level density estimator $\widehat{\rho}(\omega)$ given in Eq. (47), one runs the KPM calculation for a collection of N_s random operators $\{\hat{F}_{i_s}\}_{i_s=1}^{N_s}$. After obtaining the collection of coefficients: $\{(\mu_n(\hat{F}_{i_s}))_{n=0}^{2N_{\text{it}}}\}_{i_s=1}^{N_s}$, the QRPA level density estimator

is given by

$$\widehat{\rho}(\omega) = N_p \frac{\sum_{n=0}^{2N_{\text{it}}} \overline{\mu_n(\hat{F}_{i_s})} \frac{2/\pi}{\Omega_b \sqrt{1 - (\omega/\Omega_b)^2}} T_n\left(\frac{\omega}{\Omega_b}\right)}{\sum_{n=0}^{2N_{\text{it}}} \overline{\mu_n(\hat{F}_{i_s})} \frac{\sin\left(\frac{n\pi}{2}\right)}{\left(\frac{n\pi}{2}\right)}}, \quad (53)$$

where $\overline{\mu_n(\hat{F}_{i_s})}$ are the averaged coefficients over the collection of randomly generated samples

$$\overline{\mu_n(\hat{F}_{i_s})} = \frac{1}{N_s} \sum_{i_s=1}^{N_s} \mu_n(\hat{F}_{i_s}), \quad \forall n = 0, 1, \dots, 2N_{\text{it}}. \quad (54)$$

The KPM computation for each i_s is independent from the others and therefore can be run fully in parallel.

4.3. Spurious modes removal

In practical calculations, spurious modes, also known as the Nambu-Goldstone modes [31], often contaminate the response function due to their high transition probabilities at positive near-zero frequencies. In most nuclei, the spurious pairing $K^\pi = 0^+$, rotational $K^\pi = 1^+$ and translational $K^\pi = 0^-, 1^-$ modes in the response function will result in a corresponding spurious contribution to the calculated level density function.

The idea is to eliminate the contribution of spurious modes in the low-energy region by shifting them to high-energy region. Once the spurious mode with eigenfrequency $\Omega_1 > 0$ and eigenvector $x_1, y_1 \in \mathbb{C}^{N_p}$ is identified, the only thing that needs to be modified is the QRPA mapping (8) which now becomes

$$\begin{aligned} \begin{bmatrix} x \\ y \end{bmatrix} \mapsto & \begin{bmatrix} A & B \\ B^* & A^* \end{bmatrix} \begin{bmatrix} x \\ y \end{bmatrix} \\ & + (\widetilde{\Omega}_1 - \Omega_1) \left\{ \begin{bmatrix} +x_1 \\ -y_1 \end{bmatrix} (x^\dagger x - y^\dagger y) + \begin{bmatrix} -y_1^* \\ +x_1^* \end{bmatrix} (x_1^T y - y_1^T x) \right\}, \end{aligned} \quad (55)$$

where $\widetilde{\Omega}_1 > 0$ is the position of the shifted spurious mode. In practice most spurious modes have $\Omega_1 < 0.5$ MeV. By choosing large values of $\widetilde{\Omega}_1 > 0$, e.g. $\widetilde{\Omega}_1 \geq 200$ MeV, one can shift these modes to arbitrarily high energy. Additional details on the practical implementation of this technique are given in Appendix A.

4.4. Algorithm

Algorithm 1 summarizes the main steps of our method. The total number $\#_{\text{QFAM}}$ of FAM iterations required is

$$\#_{\text{QFAM}} = N_s N_{\text{it}} = N_s \left[\frac{1}{2} \left(\frac{\Omega_b \pi}{\sigma_{\text{KPM}}} - 1 \right) \right], \quad (56)$$

where N_{it} is obtained from Eq. (51). We emphasize again that the loop in Algorithm 1 is naturally parallelizable. For example, in the case of a non-relativistic FAM solver, if one picks $\Omega_b \approx 250$ MeV and $\sigma_{\text{KPM}} = 0.05$ MeV, it takes around $N_{\text{it}} \approx 8000$ FAM iterations per sample. If we assume that each FAM iteration lasts around ≈ 5 s, and that we can launch $N_s \approx 200$ tasks in parallel, one can expect to compute the level density function in ≈ 11 hours, which makes the method feasible in practice.

Algorithm 1: QRPA level density with FAM+KPM

Input:

- Mapping: $\begin{bmatrix} x \\ y \end{bmatrix} \in \mathbb{C}^{2N_p} \mapsto \begin{bmatrix} A & B \\ B^* & A^* \end{bmatrix} \begin{bmatrix} x \\ y \end{bmatrix} \in \mathbb{C}^{2N_p}$, provided by a FAM solver.
- Width σ_{KPM} of Gaussian approximation of Dirac delta function.
- Bounding frequency Ω_b : $\forall \Omega_i, \Omega_i \in \langle 0, +\Omega_b \rangle$.
- Optionally provide: spurious mode eigenfrequency $\Omega_1 > 0$, spurious mode eigenvector $x_1, y_1 \in \mathbb{C}^{N_p}$ and a desired position of the shifted spurious eigenfrequency $\tilde{\Omega}_1$ such that $\tilde{\Omega}_1 \in \langle 0, +\Omega_b \rangle$. How to obtain $\{\Omega_1, x_1, y_1\}$ is explained in Appendix A.
- Number of samples N_s in a collection of randomly generated excitation operators $\{\hat{F}_{i_s}\}_{i_s=1}^{N_s}$.

for $i_s = 1, 2, \dots, N_s$ **do**

- Generate a random operator \hat{F}_{i_s} defined by vectors: $\text{Re}[F_{i_s}^{20}], \text{Re}[F_{i_s}^{02}], \text{Im}[F_{i_s}^{20}], \text{Im}[F_{i_s}^{02}] \in \mathbb{R}^{N_p}$, where each component is drawn independently from $\mathcal{N}(0, \sigma^2)$.
- Compute coefficients $\mu_n(\hat{F}_{i_s})$ using spurious-corrected mapping (55) as described in Ref. [28]. The number N_{it} of FAM iterations needed is computed from Eq. (51).
- Apply the kernel transformation: $\mu_n(\hat{F}_{i_s}) \leftarrow g_n^{(2N_{\text{it}}+1)} \mu_n(\hat{F}_{i_s})$, with the Jackson kernel coefficients $g_n^{(2N_{\text{it}}+1)}$ given in Ref. [28].

end

- Compute the averaged coefficients $\overline{\mu_n(\hat{F}_{i_s})}$ as in Eq. (54).
- Using Eq. (53), evaluate $\widehat{\rho}(\omega)$ on a grid of frequencies $\omega \geq 0$, e.g., with the FFT-based method of Ref. [28].

Output:

- QRPA level density estimator $\widehat{\rho}(\omega)$ evaluated on a $\omega \geq 0$ grid.
-

5. Numerical tests

In this section, we show a series of numerical tests to evaluate the performance of the new method. We first compute the QRPA level density for synthetically generated QRPA-like matrices to illustrate the convergence of the method as we increase the number of samples N_s . We then use the open-source code `skyrme_rpa` [32] to solve the RPA equation in heavy spherical nuclei and benchmark the QRPA level density of specific K^π modes.

5.1. Examples using synthetically generated QRPA matrix

In this section we synthetically generate QRPA-like matrices A and B by employing the procedure described in Appendix B of Ref. [28]. The matrix dimension and the bounding frequency are set to $N_p = 200$ and $\Omega_b = 250$ MeV, respectively. 100 random eigenfrequencies Ω_i are generated uniformly in the range from 0 MeV to 200 MeV and combined with another 100 random eigenfrequencies Ω_i generated uniformly in the range from 0 MeV to 30 MeV, with the intent of making the resulting QRPA spectrum more dense in the low energy region.

Next, we generate a uniformly random sequence of values $\theta_1, \dots, \theta_{N_p}$ in the interval $[0, \theta_{\text{max}}]$, and two unitary matrices $C, D \in \mathbb{C}^{N_p \times N_p}$ as Q factors in the QR decomposition of two random $N_p \times N_p$ complex matrices. The X and Y matrices are

constructed as

$$X = D \text{diag} [\cosh \theta_i]_{i=1}^{N_p} C \quad \text{and} \quad Y = D^* \text{diag} [\sinh \theta_i]_{i=1}^{N_p} C, \quad (57)$$

and then used to generate the QRPA matrices A and B as

$$A = +X\Omega X^\dagger + (Y\Omega Y^\dagger)^* \quad \text{and} \quad B = -X\Omega Y^\dagger - (X\Omega Y^\dagger)^T. \quad (58)$$

Note that the parameter θ_{max} determines the magnitudes of $\|Ye_i\|^2$ and therefore the corresponding theoretical relative error ε_i in the limit $N_s \rightarrow +\infty$, according to Eq.(42).

We set the width for the Gaussian approximation of the Dirac delta function equal to $\sigma_{\text{KPM}} = 0.05$ MeV, which for $\Omega_b = 250$ MeV according to Eq. (56) corresponds to the number $N_{\text{it}} \approx 8000$ of QFAM iterations needed in the KPM method. We draw the components of vectors $F_{i_s}^{20}, F_{i_s}^{02} \in \mathbb{C}^{N_p}$ according to Eq. (22) with a standard deviation of $\sigma = 1$ MeV. Recall that the error on the estimator $\widehat{\rho}(\omega)$ is independent of the value of σ . Figure 1 shows the level density $\rho(\omega)$ and its estimator $\widehat{\rho}(\omega)$ computed for a very large number of samples $N_s = 5000$ and $\theta_{\text{max}} = 0.5$.

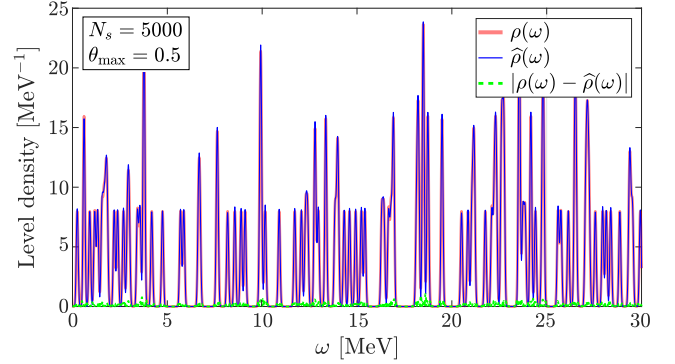


Figure 1: Comparison of the level density function $\rho(\omega)$ and its estimator $\widehat{\rho}(\omega)$ computed for a very large number of samples $N_s = 5000$ and $\theta_{\text{max}} = 0.5$. $\rho(\omega)$ is calculated by approximating the Dirac delta function with a Gaussian function, using a standard deviation of σ_{KPM} .

5.1.1. Example with fixed θ_{max} and varying N_s

In this subsection we fix the value $\theta_{\text{max}} = 1$ and vary the number of randomly generated excitation operators $N_s = 50, 200, 800$. In Fig. 2 we show the obtained relative error evaluated at QRPA eigenfrequencies $\omega = \Omega_i$ between the level density estimator $\widehat{\rho}(\omega)$ compared to the true level density function $\rho(\omega)$ when the Dirac delta function in Eq. (1) is replaced by a Gaussian with standard deviation of σ_{KPM} . Figure 2 also shows the theoretical relative error limit ε_i in the case of an infinitely large collection of random excitation operators $N_s \rightarrow +\infty$ as defined in Eq. (41). We can see that for $N_s = 800$, the obtained relative error is of the same order $\approx 5 - 10\%$ as the theoretical limit. Therefore, if $\theta_{\text{max}} \approx 1$, a few hundreds of randomly generated excitation operators are enough to give an estimate up to $\approx 10\%$ relative error. We remind the reader that (42) and (43) hold in the limit of an infinitesimally small width of Dirac delta functions and the $N_s \rightarrow +\infty$ limit. When using a finite-width approximation of the Dirac delta function and a finite number of samples N_s , these relations are only approximately valid.

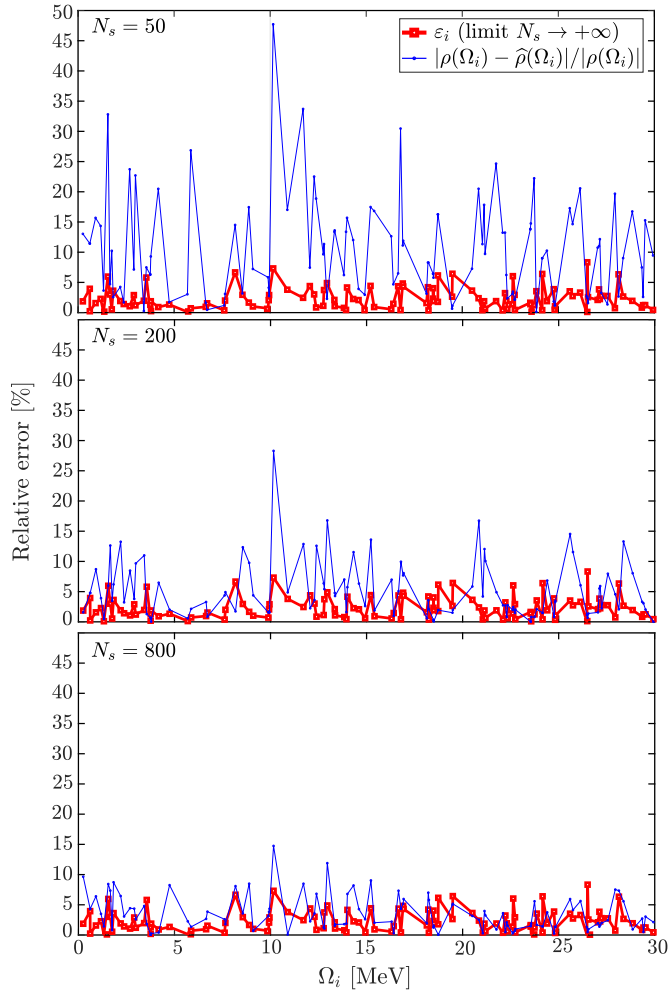


Figure 2: The blue curve with plain circles shows a relative error evaluated at eigenfrequencies $\omega = \Omega_i$ between the level density $\rho(\omega)$ and its estimator $\widehat{\rho}(\omega)$ computed using $N_s = 50, 200$ and 800 randomly generated excitation operators and $\theta_{\max} = 1$. The red curve with open squares shows the theoretical relative error ε_i in the $N_s \rightarrow +\infty$ limit.

5.1.2. Example with fixed N_s and varying θ_{\max}

In this subsection we fix the number of samples N_s to a very large value $N_s = 5000$ and vary the parameter $\theta_{\max} = 0.5, 1.0, 2.0$. Recall that small values of θ_{\max} correspond to small values of the matrix elements of Y , hence a smaller error ε_i owing to Eq. (41). Like in the previous subsection, in Fig. 3 we compare the level density estimator $\widehat{\rho}(\omega)$ with the true level density $\rho(\omega)$ by showing the theoretical relative error limit ε_i and the computed relative error $|\widehat{\rho}(\omega) - \rho(\omega)|/|\rho(\omega)|$ at $\omega = \Omega_i$. We first notice that as the value of θ_{\max} is reduced, the theoretical relative error limit ε_i is reduced indeed. Secondly, even for a large number of samples $N_s = 5000$, the computed relative error is primarily dominated by statistical errors due to the variations within the finite size of the collection of random samples, rather than the theoretical error limit. This implies that even under the most favorable condition of $\theta_{\max} = 0$, the resulting error would be approximately 5%, even with a very large sample size of $N_s = 5000$.

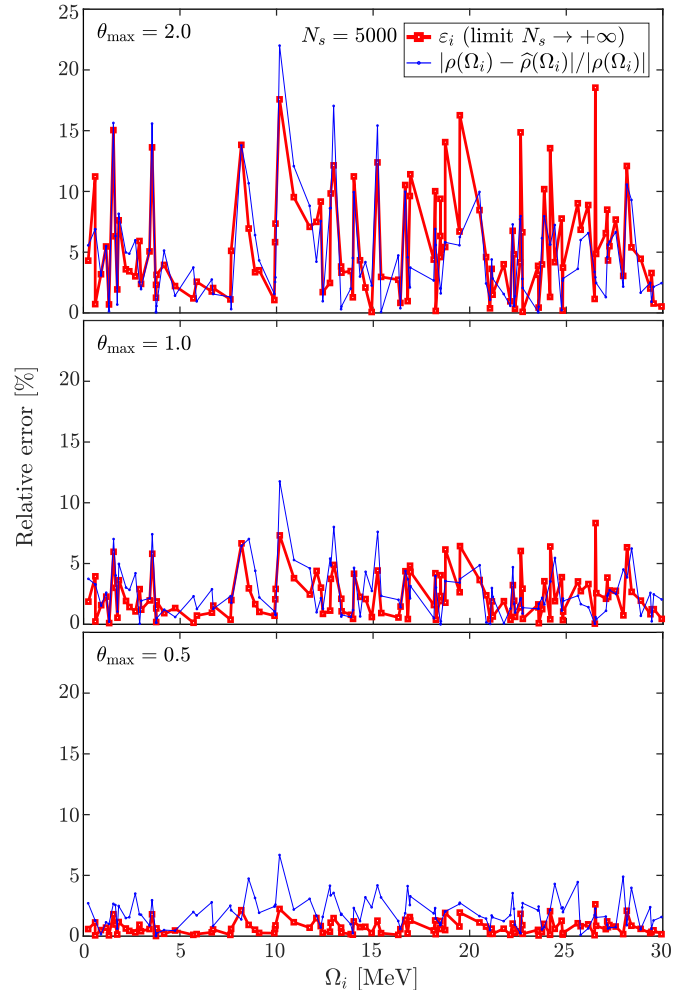


Figure 3: The blue curve with plain circles shows a relative error evaluated at eigenfrequencies $\omega = \Omega_i$ between the level density $\rho(\omega)$ and its estimator $\widehat{\rho}(\omega)$ computed using a very large number $N_s = 5000$ of randomly generated excitation operators and $\theta_{\max} = 0.5, 1.0, 2.0$. The red curve with open squares shows the theoretical relative error ε_i in the $N_s \rightarrow +\infty$ limit.

5.2. Examples using matrix RPA code `skyrme_rpa`

In this section, we validate the proposed method with the realistic RPA solver `skyrme_rpa` [32]. This solver is implemented for closed shell spherical nuclei with Skyrme-type interactions. The Hartree-Fock equations are solved on a radial mesh using box boundary conditions and the RPA matrix is explicitly constructed and diagonalized for a given value of total angular momentum and parity J^π .

We have modified the `skyrme_rpa` code to extract explicitly the matrices A and B for given J^π with the intent of using them rather than synthetically generated ones as was done in the previous section. This shall provide an insight of realistic values for Ω_i and θ_i which were previously randomly generated. We use the desired width $\sigma_{\text{KPM}} = 0.05$ MeV, bounding frequency $\Omega_b = 250$ MeV, and standard deviation of randomly generated excitation operators $\sigma = 1$ MeV. Guided by the previous synthetic examples, we choose the number of samples $N_s = 500$ as a compromise between computational complexity and statistical fluctuations.

5.2.1. $J^\pi = 5^-$ level density of ^{120}Sn

We use the same numerical setup as in Section 4.2 of Ref. [28]. Calculations were performed by employing the SLy5 Skyrme interaction on ^{120}Sn in a 20 fm radius box with 0.1 fm radial step and 100 MeV cutoff energy; see Ref. [32] for details. The resulting RPA matrix for $J^\pi = 5^-$ is of order $N_p = 1310$. First we solve the QRPA eigenvalue problem as in Eqs. (3) and (4) and obtain the eigenfrequencies Ω_i , and matrices X, Y . The values of $\theta_1, \dots, \theta_{N_p}$ are obtained by computing the singular values of either X or Y matrix. The maximum angle obtained is equal to: $\max_{i=1, \dots, N_p} \theta_i = 0.38$. As demonstrated in the previous section, this a favourable scenario regarding the theoretical error ε_i in the $N_s \rightarrow +\infty$ limit. In Fig. 4 we compare the computed level density estimator against the true function. We notice that the obtained relative error is the largest for the eigenmode with the lowest eigenfrequency. This is expected because this mode has the highest ground-state correlation energy and therefore the largest $\|Y\mathbf{e}_i\|^2$, which yields largest ε_i . Other than the lowest mode, the obtained relative error is of order 5 – 10% for other modes, and is mostly influenced by statistical fluctuations.

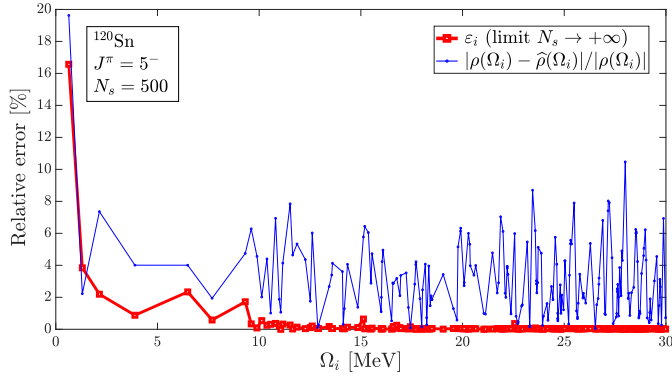


Figure 4: Theoretical relative error ε_i in the limit $N_s \rightarrow +\infty$ and computed relative error: $|\rho(\Omega_i) - \widehat{\rho}(\Omega_i)|/|\rho(\Omega_i)|$ for $J^\pi = 5^-$ states in ^{120}Sn . Calculations were performed with $N_s = 500$ randomly generated excitation operators; see text for details about the RPA calculation.

5.2.2. $J^\pi = 1^-$ level density of ^{208}Pb

In this example we use the SLy5 Skyrme interaction on ^{208}Pb in a box of radius 24 fm with 0.1 fm radial step and 100 MeV cutoff energy. The resulting RPA matrix for $J^\pi = 1^-$ is of order $N_p = 1394$. In this case, the maximum angle θ_i is equal to: $\max_{i=1, \dots, N_p} \theta_i = 1.08$, which is why we expect a somewhat larger error than in the previous example. The top panel of Fig. 5 shows the comparison between the computed level density estimator and the correct level density function. The low-lying spurious 1^- mode is at $\Omega_1 \approx 1$ MeV.

In the middle panel of Fig. 5, we plot the theoretical relative error ε_i in the limit $N_s \rightarrow +\infty$ and the computed relative error $|\rho(\Omega_i) - \widehat{\rho}(\Omega_i)|/|\rho(\Omega_i)|$. We notice that the low-lying spurious 1^- mode yields a very large relative error. This is expected because such spurious modes have a very large norm $\|Y\mathbf{e}_i\|^2$ and consequently large relative error ε_i in the $N_s \rightarrow +\infty$ limit; see Eq. (41). In this particular case, $\varepsilon_i = 334\%$ for the spurious mode.

In order to eliminate the contribution of the spurious mode

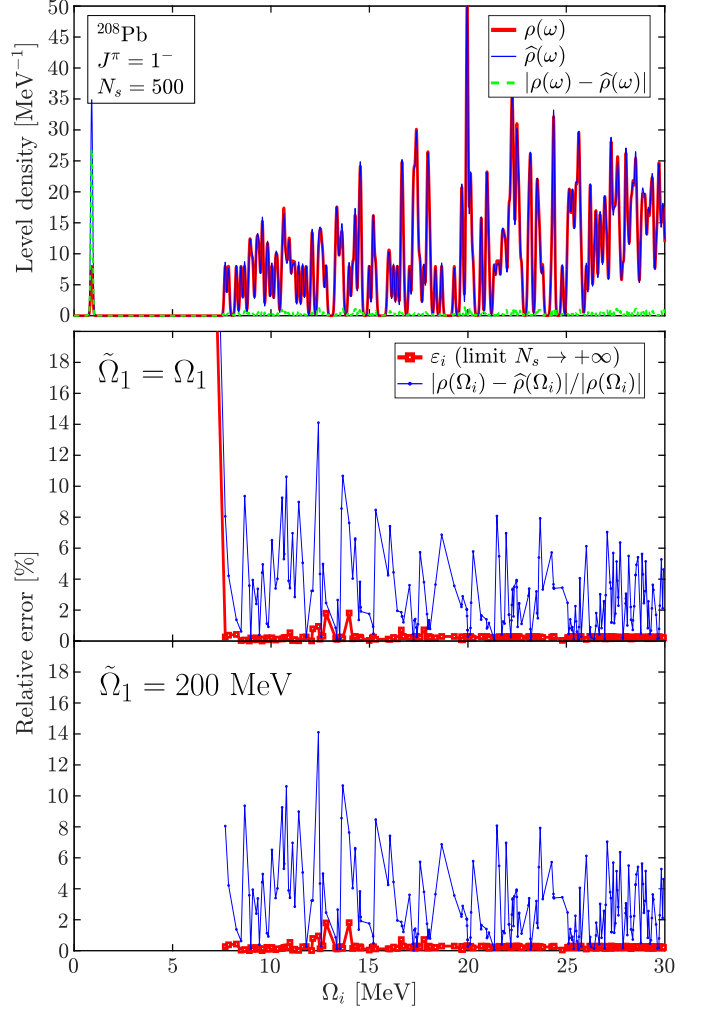


Figure 5: Top panel: Level density estimator $\widehat{\rho}(\omega)$, true density $\rho(\omega)$ and absolute difference of the two for $J^\pi = 1^-$ states in ^{208}Pb as a function of the energy ω . Calculations were performed for $N_s = 500$ samples. Middle panel: Relative difference between $\widehat{\rho}(\omega)$ and $\rho(\omega)$ and a theoretical relative error limit ε_i as a function of the energy Ω_i of the RPA eigenstate. Bottom panel: Same as middle panel after moving the spurious mode to $\Omega_1 = 200$ MeV with the procedure described in Appendix A.

to the level density in the low-energy region, we follow the method outlined in Appendix A and shift the spurious mode to high energy $\widetilde{\Omega}_1 = 200$ MeV. The bottom panel of Fig. 5 shows the relative error after this operation. Now the obtained relative error is of order 5 – 10% and is mostly influenced by statistical fluctuations.

6. Conclusion

In this work, we have proposed a new method to approximate the QRPA level density, that is, the density of vibrational states that result from the diagonalization of the QRPA matrix. Our approach relies on using the Finite Amplitude Method to compute the linear responses for a collection of random excitation operators that probe the QRPA spectrum. While the error on the level density decreases with the number of random operators, i.e. the number of samples, we derive a theoretical rela-

tive error bound in the case of infinite number of samples. This bound is expected to be relatively small; at the cranking approximation, it is in fact exactly zero. We use the Kernel Polynomial Method to efficiently compute the estimator of the QRPA level density. We illustrate the convergence of the method with respect to the number of samples for various magnitudes of $\|Y\|_F$ by synthetically generating QRPA-like matrices. Using publicly available RPA code, we also show that we can approximate the RPA level density to within 5–10%.

While our method is no substitute to exact diagonalization of the QRPA matrix, it offers two main advantages: (i) it is easily applicable to heavy deformed nuclei, where the cost of building the QRPA matrix can quickly become prohibitive (ii) computationally, it is a naturally parallel problem since the linear response of each sample can be computed independently. The next step will be to use such QRPA level densities to compute the full level density of the nucleus by folding it with rotational bands.

7. Acknowledgements

Discussions with Tong Li are warmly acknowledged. This work was performed under the auspices of the U.S. Department of Energy by Lawrence Livermore National Laboratory under contract DE-AC52-07NA27344. Lawrence Livermore National Security, LLC. Computing support came from the Lawrence Livermore National Laboratory (LLNL) Institutional Computing Grand Challenge program.

Appendix A. Removal of spurious modes

The main idea stems from the following facts. If $H \in \mathbb{C}^{n \times n}$ is a Hermitian matrix with eigenvalues: $\lambda_1, \dots, \lambda_n \in \mathbb{R}$, and corresponding eigenvectors: $u_1, \dots, u_n \in \mathbb{C}^n$,

$$H = \sum_{i=1}^n \lambda_i u_i u_i^\dagger, \quad (\text{A.1})$$

then for any $\tilde{\lambda}_1 \in \mathbb{R}$, the updated rank-1 Hermitian matrix

$$\tilde{H} = H + (\tilde{\lambda}_1 - \lambda_1) u_1 u_1^\dagger, \quad (\text{A.2})$$

has eigenvalues: $\tilde{\lambda}_1, \lambda_2, \dots, \lambda_n \in \mathbb{R}$ and the same corresponding eigenvectors as the matrix H : $u_1, u_2, \dots, u_n \in \mathbb{C}^n$. This property can be applied to the QRPA matrix S of Eq. (2). Let us introduce a shorthand notation for the columns of the X and Y matrices of eigenvectors: $x_i = X e_i$ and $y_i = Y e_i$, for $i = 1, \dots, N_p$. For any positive $(\tilde{\Omega}_i)_{i=1}^{N_p}$, let us define the modified matrices,

$$\tilde{A} = A + \sum_{i=1}^{N_p} (\tilde{\Omega}_i - \Omega_i) \left[+x_i x_i^\dagger + (y_i y_i^\dagger)^* \right], \quad (\text{A.3})$$

$$\tilde{B} = B + \sum_{i=1}^{N_p} (\tilde{\Omega}_i - \Omega_i) \left[-x_i y_i^\dagger - (x_i y_i^\dagger)^T \right]. \quad (\text{A.4})$$

Then the new QRPA matrix where A, B are replaced by \tilde{A}, \tilde{B} still satisfies both Eqs. (3) and (4) with the same eigenvectors X

and Y only with eigenfrequencies $\tilde{\Omega}_i$ instead of Ω_i . The QRPA mapping (8) acquires the new form

$$\begin{bmatrix} x \\ y \end{bmatrix} \mapsto \begin{bmatrix} \tilde{A} & \tilde{B} \\ \tilde{B}^* & \tilde{A}^* \end{bmatrix} \begin{bmatrix} x \\ y \end{bmatrix} = \begin{bmatrix} A & B \\ B^* & A^* \end{bmatrix} \begin{bmatrix} x \\ y \end{bmatrix} + \sum_{i=1}^{N_p} (\tilde{\Omega}_i - \Omega_i) \left\{ \begin{bmatrix} x_i^\dagger x - y_i^\dagger y \\ -y_i \end{bmatrix} \begin{bmatrix} +x_i \\ -y_i \end{bmatrix} + \begin{bmatrix} x_i^T y - y_i^T x \\ +x_i^* \end{bmatrix} \begin{bmatrix} -y_i^* \\ +x_i^* \end{bmatrix} \right\}. \quad (\text{A.5})$$

In practice, we often want to shift only a single spurious mode $\Omega_1 > 0$ from near-zero value to some other value $\tilde{\Omega}_1 > 0$, away from the low-energy region we are typically interested in. If we somehow manage to obtain the eigenfrequency $\Omega_1 > 0$ of this spurious mode $\Omega_1 > 0$, then we can simply apply the formula (A.5) with $N_p = 1$ to obtain exactly the same response function but with shifted spurious mode $\Omega_1 \rightarrow \tilde{\Omega}_1$.

The question is therefore how to obtain the low-lying QRPA modes Ω_i and the corresponding (x_i, y_i) , $i = 1, \dots, k$, for a subset of k modes. There are efficient methods for computing the k eigenvalues with the smallest norm of a general matrix $H \in \mathbb{C}^{n \times n}$ which only require the inverse mapping: $x \mapsto H^{-1}x$. One such method is included in ARPACK [33], a numerical software library for solving large scale eigenvalue problems using the implicitly restarted Arnoldi method.

Consider the mapping

$$\begin{bmatrix} f^{20} \\ f^{02} \end{bmatrix} \mapsto \left(\begin{bmatrix} +I & \mathbf{0} \\ \mathbf{0} & -I \end{bmatrix} \begin{bmatrix} A & B \\ B^* & A^* \end{bmatrix} \right)^{-1} \begin{bmatrix} f^{20} \\ f^{02} \end{bmatrix}. \quad (\text{A.6})$$

According to Eq. (7), the mapping (A.6) corresponds to solving the linear response equation for zero complex frequency $\omega_\gamma = 0$ and excitation operator given by $F^{20} = -f^{20}$ and $F^{02} = +f^{02}$. This linear response equation is precisely what the FAM solves. Therefore, with the help of e.g. ARPACK, one can compute the $2k$ eigenvalues with the smallest norm: $\pm\Omega_1, \dots, \pm\Omega_k$, and the corresponding eigenvectors for the following matrix

$$\begin{bmatrix} +I & \mathbf{0} \\ \mathbf{0} & -I \end{bmatrix} \begin{bmatrix} A & B \\ B^* & A^* \end{bmatrix} \begin{bmatrix} u_i \\ v_i \end{bmatrix} = \Omega_i \begin{bmatrix} u_i \\ v_i \end{bmatrix}, \text{ for } i = 1, \dots, k. \quad (\text{A.7})$$

Recall that the eigenvalues of the QRPA matrix S of Eq. (2) come in pairs $(+\Omega_i, -\Omega_i)$ with respective eigenvectors

$$+\Omega_i : \begin{bmatrix} u_i \\ v_i \end{bmatrix}, \quad +\Omega_i : \begin{bmatrix} v_i^* \\ u_i^* \end{bmatrix}. \quad (\text{A.8})$$

Eigensolvers such as ARPACK typically normalize the eigenvector such that $\|u_i\|^2 + \|v_i\|^2 = 1$. We define the eigenvectors

$$\begin{bmatrix} x_i \\ y_i \end{bmatrix} = \frac{1}{\sqrt{\|u_i\|^2 - \|v_i\|^2}} \begin{bmatrix} u_i \\ v_i \end{bmatrix}, \text{ for } i = 1, \dots, k, \quad (\text{A.9})$$

which are normalized with respect to the QRPA metric: $\|x_i\|^2 - \|y_i\|^2 = 1$. Mathematically spurious zero-energy modes are actually non-normalizable [31], because for them $\|u_i\|^2 - \|v_i\|^2 = 0$. In practice, however, spurious modes never have exactly vanishing eigenvalue and one can normalize them.

In the case where the QRPA eigenmodes are non degenerate, two eigenvectors (A.9) for $i \neq j$, hence $\Omega_i \neq \Omega_j$, are orthogonal with respect to the QRPA metric since it is easy to show that

$$\Omega_j \begin{bmatrix} x_i \\ y_i \end{bmatrix}^\dagger \begin{bmatrix} +I & \mathbf{0} \\ \mathbf{0} & -I \end{bmatrix} \begin{bmatrix} x_j \\ y_j \end{bmatrix} = \Omega_i \begin{bmatrix} x_i \\ y_i \end{bmatrix}^\dagger \begin{bmatrix} +I & \mathbf{0} \\ \mathbf{0} & -I \end{bmatrix} \begin{bmatrix} x_j \\ y_j \end{bmatrix}. \quad (\text{A.10})$$

Therefore, for any $i, j = 1, \dots, k$, we must have

$$\begin{bmatrix} x_i \\ y_i \end{bmatrix}^\dagger \begin{bmatrix} +I & \mathbf{0} \\ \mathbf{0} & -I \end{bmatrix} \begin{bmatrix} x_j \\ y_j \end{bmatrix} = \delta_{i,j}, \quad (\text{A.11})$$

which means that eigenvectors generated from Eq. (A.9) are indeed the columns Xe_i, Ye_i of the X, Y matrices. In cases of degeneracies, the generalized Gram–Schmidt orthogonalization procedure with QRPA metric is needed in order to orthogonalize the eigenvectors $\{x_i, y_i\}$ which belong to the degenerate eigenfrequency. It is important to emphasize that the numerical accuracy of the FAM solver, namely the mapping (8), must be high enough to avoid loss of accuracy when computing the normalization factor $\sqrt{\|u_i\|^2 - \|v_i\|^2}$ in those cases where the eigenfrequency is very close to 0.

Let us also point out the importance of carefully choosing the initial vector for the iterative algorithm in libraries such as ARPACK. This comes from the fact that typical FAM solvers assume certain symmetries such as, e.g. axially symmetry, which means that only the excitation operators with certain selection rules are allowed. Typically this involves operators with well defined angular momentum K and parity π , which actually means that one works in a subspace of the QRPA matrix with well defined K^π . Therefore we also need to supply the eigensolver with an initial random vector for the mapping (A.6) that also satisfies the same selection rules as the ones of the FAM solver. In other words, the initial random vector must be an element of the appropriate K^π subspace.

In order to illustrate the method described above on a realistic example, we select the axially deformed ($\beta_2 \approx 0.5$) isotope ^{20}Ne , DD-PC1 Lagrangian and use a basis of 12 oscillator shells; see Ref. [34] for a detailed discussion of the multipole response of this isotope. We implemented the spurious mode removal method in the DIRQFAM code [35, 36] using the ARPACK eigensolver, and focus on the isoscalar $J = 2, K = 1$ response which exhibits a rotational $K^\pi = 1^+$ spurious mode.

We generated a random $K^\pi = 1^+$ excitation operator as the initial residual vector by ARPACK. This ensures that the Arnoldi algorithm implemented in ARPACK is contained within the $K^\pi = 1^+$ subspace of the QRPA matrix. We computed the response function with the KPM method and bounding frequency $\Omega_b = 4500$ MeV, a Lorentz kernel with damping parameter $\lambda = 9$ and $N_{\text{it}} = 100000$ FAM iterations. This roughly corresponds to an equivalent smearing equal to $\gamma = \Omega_b \frac{\lambda}{2N_{\text{it}}+1} \approx 0.2$ MeV; see Ref. [28] for details. In Fig. A.6 we show the computed response functions: the black curve shows the response without shifting the spurious mode, i.e. $\tilde{\Omega}_1 = \Omega_1$, the red curve shows the response when the spurious mode is shifted to $\tilde{\Omega}_1 = 40$ MeV, and the blue curve shows the response when the spurious mode is shifted to high-energy region $\tilde{\Omega}_1 = 200$

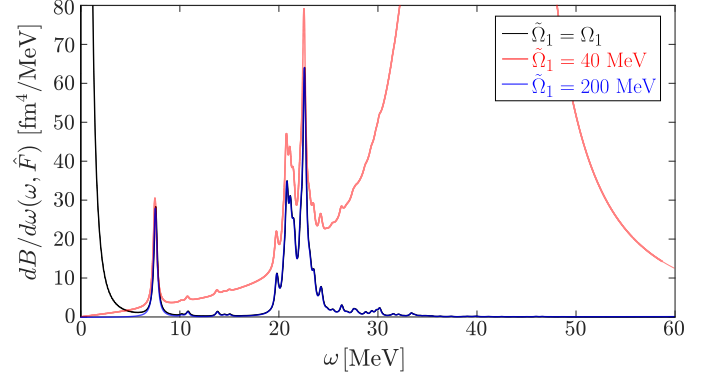


Figure A.6: Response function of ^{20}Ne for isoscalar quadrupole $J = 2, K = 1$ excitation. The black curve shows the response without spurious mode removal, the red curve shows the response when the spurious mode is shifted to $\tilde{\Omega}_1 = 40$ MeV, and the blue curve shows the response when the spurious mode is shifted to $\tilde{\Omega}_1 = 200$ MeV.

MeV. Note that even though we could shift the energy of the spurious mode to any arbitrary value $\tilde{\Omega}_i$, it should still satisfy $\tilde{\Omega}_i < \Omega_b$ for the KPM method to work.

References

- [1] H. A. Bethe, An Attempt to Calculate the Number of Energy Levels of a Heavy Nucleus, *Phys. Rev.* 50 (4) (1936) 332. doi:10.1103/PhysRev.50.332.
- [2] C. Bloch, Theory of Nuclear Level Density, *Phys. Rev.* 93 (5) (1954) 1094. doi:10.1103/PhysRev.93.1094.
- [3] T. Ericson, The statistical model and nuclear level densities, *Adv. in Phys.* 9 (36) (1960) 425. doi:10.1080/00018736000101239.
- [4] A. Bohr, B. Mottelson, *Nuclear Structure, Vol. II, Nuclear Deformations*, World Scientific, 1998. doi:10.1142/3530.
- [5] A. J. Koning, S. Hilaire, M. C. Duijvestijn, TALYS-1.0, in: *Proc. Int. Conf. Nucl. Data Sci. Technol.*, EDP Sciences, Nice, France, 2008, p. 211. doi:10.1051/ndata:07767.
- [6] M. Herman, R. Capote, B. V. Carlson, P. Obložinský, M. Sin, A. Trkov, H. Wienke, V. Zerkin, EMPIRE: Nuclear Reaction Model Code System for Data Evaluation, *Nucl. Data Sheets* 108 (12) (2007) 2655. doi:10.1016/j.nds.2007.11.003.
- [7] H. Nakada, Y. Alhassid, Total and Parity-Projected Level Densities of Iron-Region Nuclei in the Auxiliary Fields Monte Carlo Shell Model, *Phys. Rev. Lett.* 79 (16) (1997) 2939. doi:10.1103/PhysRevLett.79.2939.
- [8] M. Horoi, J. Kaiser, V. Zelevinsky, Spin- and parity-dependent nuclear level densities and the exponential convergence method, *Phys. Rev. C* 67 (5) (2003) 054309. doi:10.1103/PhysRevC.67.054309.
- [9] Y. Alhassid, G. F. Bertsch, L. Fang, Nuclear level statistics: Extending shell model theory to higher temperatures, *Phys. Rev. C* 68 (4) (2003) 044322. doi:10.1103/PhysRevC.68.044322.
- [10] H. Nakada, Y. Alhassid, Isospin-projected nuclear level densities by the shell model Monte Carlo method, *Phys. Rev. C* 78 (5) (2008) 051304. doi:10.1103/PhysRevC.78.051304.
- [11] R. A. Sen'kov, M. Horoi, High-performance algorithm to calculate spin- and parity-dependent nuclear level densities, *Phys. Rev. C* 82 (2) (2010) 024304. doi:10.1103/PhysRevC.82.024304.
- [12] R. A. Sen'kov, M. Horoi, V. G. Zelevinsky, High-performance algorithm for calculating non-spurious spin- and parity-dependent nuclear level densities, *Phys. Lett. B* 702 (5) (2011) 413. doi:10.1016/j.physletb.2011.07.004.
- [13] Y. Alhassid, M. Bonett-Matiz, S. Liu, H. Nakada, Direct microscopic calculation of nuclear level densities in the shell model Monte Carlo approach, *Phys. Rev. C* 92 (2) (2015) 024307. doi:10.1103/PhysRevC.92.024307.

- [14] S. Hilaire, J.-P. Delaroche, M. Girod, Combinatorial nuclear level densities based on the Gogny nucleon-nucleon effective interaction, *Eur. Phys. J. A* 12 (2) (2001) 169. doi:10.1007/s100500170025.
- [15] N. Schunck, *Energy Density Functional Methods for Atomic Nuclei*, IOP Expanding Physics, IOP Publishing, Bristol, UK, 2019. URL <https://doi.org/10.1088/2053-2563/aae0ed>
- [16] J. F. Berger, M. Martinot, Shell effects on state densities with given numbers of excited protons and neutrons, *Nucl. Phys. A* 226 (3) (1974) 391. doi:10.1016/0375-9474(74)90491-6.
- [17] S. Hilaire, S. Goriely, Global microscopic nuclear level densities within the HFB plus combinatorial method for practical applications, *Nucl. Phys. A* 779 (2006) 63. doi:10.1016/j.nuclphysa.2006.08.014.
- [18] S. Goriely, S. Hilaire, A. J. Koning, Improved microscopic nuclear level densities within the Hartree-Fock-Bogoliubov plus combinatorial method, *Phys. Rev. C* 78 (6) (2008) 064309. doi:10.1103/PhysRevC.78.064309.
- [19] S. Hilaire, M. Girod, S. Goriely, A. J. Koning, Temperature-dependent combinatorial level densities with the DIM Gogny force, *Phys. Rev. C* 86 (6) (2012) 064317. doi:10.1103/PhysRevC.86.064317.
- [20] S. Hilaire, S. Goriely, S. Péru, G. Gosselin, A new approach to nuclear level densities: The QRPA plus boson expansion, *Phys. Lett. B* 843 (2023) 137989. doi:10.1016/j.physletb.2023.137989.
- [21] J. Terasaki, J. Engel, Self-consistent Skyrme quasiparticle random-phase approximation for use in axially symmetric nuclei of arbitrary mass, *Phys. Rev. C* 82 (3) (2010) 034326. doi:10.1103/PhysRevC.82.034326.
- [22] M. Martini, S. Péru, S. Hilaire, S. Goriely, F. Lechaftois, Large-scale deformed quasiparticle random-phase approximation calculations of the γ -ray strength function using the Gogny force, *Phys. Rev. C* 94 (1) (2016) 014304. doi:10.1103/PhysRevC.94.014304.
- [23] T. Nakatsukasa, T. Inakura, K. Yabana, Finite amplitude method for the solution of the random-phase approximation, *Phys. Rev. C* 76 (2) (2007) 024318. doi:10.1103/PhysRevC.76.024318.
- [24] P. Avogadro, T. Nakatsukasa, Finite amplitude method for the quasiparticle random-phase approximation, *Phys. Rev. C* 84 (1) (2011) 014314. doi:10.1103/PhysRevC.84.014314.
- [25] P. Ring, P. Schuck, *The Nuclear Many-Body Problem*, Texts and Monographs in Physics, Springer, 2004.
- [26] E. Di Napoli, E. Polizzi, Y. Saad, Efficient estimation of eigenvalue counts in an interval, *Numerical Linear Algebra with Applications* 23 (4) (2016) 674–692. doi:<https://doi.org/10.1002/nla.2048>.
- [27] L. Lin, Y. Saad, C. Yang, Approximating spectral densities of large matrices, *SIAM Rev.* 58 (1) (2016) 34–65. doi:10.1137/130934283.
- [28] A. Bjelčić, T. Nikšić, Z. Drmač, Chebyshev kernel polynomial method for efficient calculation of the quasiparticle random phase approximation response function, *Comput. Phys. Commun.* 280 (2022) 108477. doi:10.1016/j.cpc.2022.108477.
- [29] N. Hinohara, M. Kortelainen, W. Nazarewicz, Low-energy collective modes of deformed superfluid nuclei within the finite-amplitude method, *Phys. Rev. C* 87 (6) (2013) 064309. doi:10.1103/PhysRevC.87.064309.
- [30] J. Toivanen, B. G. Carlsson, J. Dobaczewski, K. Mizuyama, R. R. Rodríguez-Guzmán, P. Toivanen, P. Veselý, Linear response strength functions with iterative Arnoldi diagonalization, *Phys. Rev. C* 81 (2010) 034312. doi:10.1103/PhysRevC.81.034312. URL <https://link.aps.org/doi/10.1103/PhysRevC.81.034312>
- [31] N. Hinohara, Collective inertia of the Nambu-Goldstone mode from linear response theory, *Phys. Rev. C* 92 (3) (2015) 034321. doi:10.1103/PhysRevC.92.034321.
- [32] G. Colò, L. Cao, N. Van Giai, L. Capelli, Self-consistent RPA calculations with Skyrme-type interactions: The `skyrme_rpa` program, *Comput. Phys. Commun.* 184 (1) (2013) 142. doi:10.1016/j.cpc.2012.07.016.
- [33] R. B. Lehoucq, D. C. Sorensen, C. Yang, *ARPACK Users' Guide*, Society for Industrial and Applied Mathematics, 1998. doi:10.1137/1.9780898719628. URL <https://epubs.siam.org/doi/abs/10.1137/1.9780898719628>
- [34] F. Mercier, A. Bjelčić, T. Nikšić, J.-P. Ebran, E. Khan, D. Vretenar, Low-energy cluster modes in $N=Z$ nuclei, *Phys. Rev. C* 103 (2) (2021) 024303. doi:10.1103/PhysRevC.103.024303.
- [35] A. Bjelčić, T. Nikšić, Implementation of the quasiparticle finite amplitude method within the relativistic self-consistent mean-field framework: The program DIRQFAM, *Comput. Phys. Commun.* 253 (2020) 107184. doi:10.1016/j.cpc.2020.107184.
- [36] A. Bjelčić, T. Nikšić, Implementation of the quasiparticle finite amplitude method within the relativistic self-consistent mean-field framework (II): The program DIRQFAM v2.0.0, *Comput. Phys. Commun.* 287 (2023) 108689. doi:10.1016/j.cpc.2023.108689.